RESEARCH ARTICLE | FEBRUARY 08 2023

Amplitude modulation of velocity fluctuations in the atmospheric flows over real urban morphology

Yixun Liu (刘乂汛) ; Chun-Ho Liu (廖俊豪) ; Guy P. Brasseur ; Christopher Y. H. Chao (趙汝恒)

Physics of Fluids 35, 025116 (2023)
https://doi.org/10.1063/5.0135475

Physics of Fluids ARTICLE scitation.org/journal/phf

Amplitude modulation of velocity fluctuations in the atmospheric flows over real urban morphology

Cite as: Phys. Fluids **35**, 025116 (2023); doi: 10.1063/5.0135475
Submitted: 19 November 2022 · Accepted: 14 January 2023 ·
Published Online: 8 February 2023

Yixun Liu (刘乂汛),[1] Chun-Ho Liu (廖俊豪),[1,a)] Guy P. Brasseur,[2,3,4] and Christopher Y. H. Chao (趙汝恒)[5,6]

AFFILIATIONS

[1]Department of Mechanical Engineering, The University of Hong Kong, Hong Kong
[2]Department of Civil and Environmental Engineering, The Hong Kong Polytechnic University, Hung Hom, Kowloon, Hong Kong
[3]National Center for Atmospheric Research, Boulder, Colorado 80305, USA
[4]Max Planck Institute for Meteorology, Hamburg, Germany
[5]Department of Building Environment and Energy Engineering, The Hong Kong Polytechnic University, Hung Hom, Kowloon, Hong Kong
[6]Department of Mechanical Engineering, The Hong Kong Polytechnic University, Hung Hom, Kowloon, Hong Kong

[a)]**Author to whom correspondence should be addressed:** liuchunho@graduate.hku.hk.
Tel.: +852 3917 7901/+852 9788 7951. **Fax:** +852 2858 5415. **URL:** https://aplhk.tech

ABSTRACT

Amplitude modulation (AM) quantifies the top-down interactions between the large-scale motions (LSMs) in the outer layer and the near-ground turbulence structures. They are important to the momentum transport and pollutant dispersion in urban atmospheric surface layers (ASLs). The dataset of large-eddy simulation over a densely built region in Kowloon Peninsula, Hong Kong, therefore, is adopted to investigate the AM of small-scale eddies by LSMs in the ASL over real urban morphology. Alike its smooth-wall counterpart, the small-scale eddies are (positively) amplitude modulated by the LSMs in most regions of the roughness sublayer (RSL). However, negative AM is unexpectedly found in the RSL on the building windward side in this study, illustrating the heterogeneity of the urban surface and the flow dynamics being affected aloft. In addition, strong sweep ($u' > 0$ and $w' < 0$) and ejection ($u' < 0$ and $w' > 0$) dominate the flows, respectively, in the positive and negative AM zones. In the positive AM zones, the large-scale sweep (${u_L}' > 0$) leads to the surplus in the small-scale turbulence kinetic energy (TKE), while the large-scale ejection (${u_L}' < 0$) brings a TKE deficit to the small-scale eddies. By contrast, the large-scale sweeps result in a TKE deficit to the small-scale eddies and the large-scale ejections result in a TKE surplus in the negative AM zones. These findings could help elucidate the AM over different building designs and urban morphology in cities, promoting the momentum transport and pollutant dispersion via proper city planning.

I. INTRODUCTION

In recent years, air pollution has undoubtedly been recognized as a serious, worldwide public health concern that is related to millions of premature deaths annually (Forouzanfar *et al.*, 2016, Shrivastava *et al.*, 2016). In cities, rapid industrialization and urbanization have often led to poor air quality, significantly incurring the risk of physical and psychological affliction. Industrial emissions, vehicular exhaust, cooking effluent, and heating discharge are the primary sources of air pollutants in metropolis; the situation is unfortunately exacerbated by dense buildings and imperfect urban design. Moreover, the elevated concentrations of aerosols in cities are arousing public worry about the respiratory disease (Rowe *et al.*, 2021, Farkas *et al.*, 2022). Felicitous urban planning helps remediate the environmental influence from/on ill-protected buildings such as infectious disease hospitals (source) or schools and retirement homes (vulnerable groups; Alirol *et al.*, 2011, Lee *et al.*, 2020).

The wind is the basic driving force for pollutant dilution, aerosol removal, and thermal comfort. However, the massive constructions in urban areas slow down the winds tacitly that, in turn, weakens ground-level ventilation. In particular, a (thin) roughness sublayer (RSL) is developed over the buildings and below the (conventional) inertial sublayer (ISL). The rather homogeneous ISL dynamics are well

described by the Monin–Obukhov similarity theory (MOST). Whereas, RSL winds and turbulence are inhomogeneous in response to individual buildings (Giometto *et al.*, 2016, Li *et al.*, 2019). The small-scale, wall-attached RSL eddies shelter the urban canopy layers (UCLs) from the entrainment of large-scale eddies from the ISL (or even the outer layer), suppressing the local transport of heat, mass, and momentum (Wang *et al.*, 2016).

The studies of turbulence structures in atmospheric surface layers (ASLs) originated from the experiments and simulations of the flows over smooth walls (Kline *et al.*, 1967, Corino *et al.*, 1969, and Lu *et al.*, 1973) and idealized urban morphology (Raupach, 1981, Bandyopadhyay *et al.*, 1988, Bisset *et al.*, 1991, and Coceal *et al.*, 2007). With the recent advancement in model fabrication, measurement techniques, and computation science, the flows over real urban surfaces have been described in detail through wind tunnel experiments (Perret *et al.*, 2018, Bross *et al.*, 2019, and Mo *et al.*, 2021), field measurements (Lotfy *et al.*, 2019, Li *et al.*, 2021), and large-eddy simulations (LESs; Inagaki *et al.*, 2017, Salesky *et al.*, 2018, Auvinen *et al.*, 2020, and Yao *et al.*, 2022). The ASL turbulence structures exhibit a wide range of motion scales. In particular, some latest studies have unveiled the existence of large-scale motions (LSMs) with rather high energy as well as efficient transport (Li *et al.*, 2019, Auvinen *et al.*, 2020, Wu *et al.*, 2020, and Lin *et al.*, 2021). For example, the footprint of high-speed ASL LSMs was detected in direct numerical simulation (DNS) (Agostini *et al.*, 2018) and LES (Liu *et al.*, 2023a, 2023b). These large-scale structures, whose (streamwise) wavelength λ_x could be up to ten times the thickness of the turbulent boundary layer (TBL) δ, contain a large portion of the turbulence kinetic energy (TKE) in the outer layer. Their transport is more efficient than that of the small-scale ones. In addition, very large-scale motions (VLSMs; extending to over 20δ in length) were found populating the logarithmic region of TBLs (Hutchins *et al.*, 2007a). They leave a footprint in the near-ground regions and even UCLs where small-scale eddies dominate.

The momentum transfer and pollutant transport in street canyons are complicated by the wide spectrum of eddy structures associated with heterogeneous buildings (Mo *et al.*, 2021). Because of the less efficient transport of small-scale eddies in street canyons (Wang *et al.*, 2016, Li *et al.*, 2019), the LSMs (and their interaction with the small eddies in street canyons) have drawn research attention because the VLSM entrainment from the outer layer could substantially enhance the local turbulence level to improve the street-canyon transport efficiency (Mathis *et al.*, 2009, Bernardini *et al.*, 2011, Mathis *et al.*, 2011, Perret *et al.*, 2013, Talluru *et al.*, 2014, Tang *et al.*, 2019, and Kim *et al.*, 2020). For example, it was reported that the small-scale flow structures in the near-ground region are subject to a high degree of amplitude modulation (AM) from much larger-scale motions (Mathis *et al.*, 2009). In other words, the amplitude of small-scale signals increases and decreases, respectively, with the positive and negative fluctuations of large-scale signals. More specifically, the large regions of streamwise momentum deficit (associated with the low-speed footprint of the VLSMs) are accompanied by reduced small-scale fluctuations in the near-wall region. In contrast, for large-scale, high-momentum fluids, the small-scale fluctuating component is more energetic (Hutchins *et al.*, 2007b). Afterward, two-point AM correlation demonstrated that these LSMs from the TBL core regions impose a top-down interaction between the outer layer and the near-ground region (Bernardini *et al.*, 2011). Moreover, (the amplitudes of) all the components of fluctuating velocity and momentum flux are modulated in a manner similar to that of the streamwise fluctuating velocity (u'; Talluru *et al.*, 2014). These studies have advanced our understanding of near-ground turbulence structures and dynamics together with the energy budget.

Lately, the influence of (individual) buildings on AM has drawn keen attention. By explicitly resolving the roughness elements, it was shown that large-scale fluctuating velocities exhibit stronger AM on both the small and dissipative scales in the near-ground regions (Tang *et al.*, 2018). In addition, the perturbation induced by the roughness elements shortens the time shifts between small-scale variations (amplitude and frequency) and large-scale fluctuations. These findings elucidate the interaction between the near-ground region and the outer layer, shedding some light on the potential of promoting near-ground (vertical) transport by AM over urban areas.

Although concerted effort has been sought, most AM studies available in the literature have been based on either smooth wall or arrays of identical, idealized roughness elements. Our understanding of AM in the flows over real urban morphology (complex rough surfaces) is rather limited. It, in turn, hinders the exploitation of the aforementioned highly efficient, energetic VLSMs (in the outer layer) from enhancing the pedestrian-level ventilation. Cities are characterized by building clusters with different shapes, layouts, and orientations (Auvinen *et al.*, 2020, Mo *et al.*, 2021, and Yao *et al.*, 2022) which would impose diversified effects on the AM. Hence, there is a need to investigate the roles of heterogeneous urban surfaces in AM and the subsequent influence on transport processes. To the best knowledge of the authors, this paper is the first attempt to investigate the AM in the ASLs over real urban morphology.

In this study, the LES dataset over a densely built downtown area in Kowloon Peninsula, Hong Kong, is adopted to compare the AM between smooth and real-urban surfaces. The influence of heterogeneous buildings is critically examined that unveils certain negative AM zones in the RSL (near the buildings and ground) for the first time. The dissimilar flow patterns (ejection $Q2$ and sweep $Q4$) in positive and negative AM zones are further compared by the joint probability density function (JPDF) of streamwise (u') and vertical (w') fluctuating velocities which could be used to investigate the flow anisotropy (Reuther *et al.*, 2020). By the JPDF sampled at different scales, the key contributors to the flow anisotropy and asymmetry are identified. Finally, the spatiotemporal conditional sampling reveals how the (positive and negative) AM influences the TKE of small-scale eddies in response to large-scale ejection $Q2$ and sweep $Q4$ events over real urban morphology.

II. METHODOLOGY

A. Governing equation

LES of isothermal and incompressible flows is adopted in our work. There is no doubt that thermal stratification in urban ASLs is important (Barlow, 2014, Aliabadi *et al.*, 2019). Hence, thermal conditions, such as urban heat island, will be considered in our future work. The principal idea behind LES is to reduce the complexity by modeling the smallest turbulence length scales, which are isotropic but most computationally expensive to resolve, via spatially filtering the Navier–Stokes equations. As such, the equations governing the conservation of mass and momentum in resolved scales are

$$\frac{\partial \widetilde{u}_m}{\partial x_m} = 0 \tag{1}$$

and

$$\frac{\partial \widetilde{u}_m}{\partial t} + \frac{\partial}{\partial x_n}\widetilde{u}_m\widetilde{u}_n = -\frac{\partial \widetilde{p}}{\partial x_m} - \frac{\partial \tau_{mm}}{\partial x_m} - \frac{\partial \tau_{mn}}{\partial x_n}, \tag{2}$$

respectively, where overtilde $\widetilde{\psi}$ denotes the spatial filter for LES resolved scales, $\widetilde{u}_m$ is the resolved-scale velocity vector, and t is the time. The summation convention on repeated indices (m, $n = 1$, 2, and 3) applies. Hence, $\widetilde{u}$, $\widetilde{v}$, and $\widetilde{w}$ are the resolved-scale velocity components in the streamwise (x), spanwise (y), and vertical (z) direction of Cartesian coordinates, respectively. Moreover, $\widetilde{p}$ is the resolved-scale kinematic pressure and

$$\tau_{mn} = \widetilde{u_m u_n} - \widetilde{u}_m\widetilde{u}_n = -\nu_{SGS}\left(\frac{\partial \widetilde{u}_m}{\partial x_n} + \frac{\partial \widetilde{u}_n}{\partial x_m}\right) + \frac{2}{3}k_{SGS}\delta_{mn}, \tag{3}$$

the (unresolvable) anisotropic component of subgrid-scale (SGS) momentum flux which is modeled by the Smagorinsky model (Smagorinsky, 1963) as a common approach in atmospheric boundary layer modeling (Aliabadi *et al.*, 2018, Ahmadi-Baloutaki *et al.*, 2021). Here, δ_{mn} is the Kronecker delta,

$$\nu_{SGS} = C_k k_{SGS}^{1/2}\Delta \tag{4}$$

is the SGS kinematic viscosity, C_k (=0.07) is the Smagorinsky constant, Δ ($= \Delta\Omega^{1/3}$) is the LES filter width (Deardorff, 1970), and $\Delta\Omega$ is the volume of the computation cell. In addition, the one-equation SGS TKE model,

$$\frac{\partial k_{SGS}}{\partial t} + \frac{\partial}{\partial x_m}k_{SGS}\widetilde{u}_m = -\frac{1}{2}\tau_{mn}\frac{\partial \widetilde{u}_m}{\partial x_n} + \frac{\partial}{\partial x_m}\left(\nu_{SGS}\frac{\partial k_{SGS}}{\partial x_m}\right) - C_\varepsilon\frac{k_{SGS}^{3/2}}{\Delta}, \tag{5}$$

is adopted to ensure SGS TKE conservation (Cheng and Yang, 2023). Here, C_ε (=1.05) is a model constant for SGS TKE dissipation (Yoshizawa *et al.*, 1985).

B. Numerical method

The governing equations are solved by the finite volume method (FVM) of OpenFOAM-V1806 (OpenFOAM, 2022). The conservation of momentum is integrated in the time domain by the implicit, second-order-accurate backward differencing. The gradient and the divergence terms are solved, respectively, by the second-order-accurate Gaussian FVM integration of cell-limited gradient scheme and the limited linear divergence schemes. The PIMPLE algorithm (OpenFOAM, 2022) is implemented to handle the pressure–velocity coupling. The preconditioner is the geometric algebraic multigrid (GAMG) method. Afterward, the pressure is solved by the conjugate gradient (CG) method. Other variables are solved by the bi-conjugate gradient (PBiCG) method. The convergence criterion is the residual less than 10^{-8} between two steps of the Krylov iteration. The mathematical model is integrated for 6000 s for initialization. After the flow reaches a quasi-steady state, another 7200 s ($=100H_{ave}/u_\tau$) are recorded that is long enough to ensure statistical convergence (Bernardini *et al.*, 2014, Vinuesa *et al.*, 2016). Here, H_{ave} (= 36 m) is the mean building height and u_τ (=0.59 m s^{-1}) is the friction velocity across the entire spatial domain.

C. Computation domain and boundary conditions

The computation domain features a highly detailed description of a densely built downtown area in Kowloon Peninsula, Hong Kong [Fig. 1(a)]. It is discretized by 9.1 × 10^6 finite volume (FV) cells [Fig. 1(b)]. The streamwise (x), spanwise (y), and vertical (z) extent is L_x (=5440 m), L_y (= 1230 m), and L_z (= 2000 m), respectively. The prevailing mean wind speed in the entire domain is less than 10 m s^{-1}. The characteristic size Δ ($= \Delta\Omega^{1/3}$) of individual FV cells varies from 0.65 to 60 m, so the time step is set to $\Delta t = 0.02$ s to fulfill the Courant–Friedrichs–Lewy (CFL) criteria (CFL number less than unity). A grid stretching from 1:2 to 1:4 is implemented to the near-ground region to refine the spatial resolution. In the near-ground regions ($z \leq 100$ m), the characteristic mesh spacing Δ ($= \Delta\Omega^{1/3}$, where $\Delta\Omega$ is the volume of computation cell) is around 3 m, whose 5%, 50%, and 95% percentiles are 3.08, 3.81, and 4.22 m, respectively. This spatial resolution also fulfills one of the practical guidelines (Tominaga *et al.*, 2008) that is 1/10 of the building length scale (mean height H_{ave} = 36 m in the current case) in the near-ground regions. The dimensionless size of the mesh next to the building facades y^+ ($=\Delta \times u_w/\nu$ =_(3 m × 0.02 m s^{-1})/1.557 × 10^{-5} m^2 s^{-1} = 3.85 × 10^3, where u_w [$= (\tau_w/\rho)^{1/2} = 0.02$ m s^{-1}] is the friction velocity, ν is the kinematic viscosity, τ_w is the wall shear stress, and ρ is the air density) is close to 4000 that falls within the logarithmic regions (Pope *et al.*, 2000). The current wall function follows Spalding (1962), that is, applicable in entire laminar and turbulent flow regimes in view of the infinitely high Reynolds number in practical flows.

The inlet boundary condition (BC) of wind speeds is given by

$$\widetilde{u} = U_s \times \left(\frac{z}{z_s}\right)^{1/5} \quad \text{and} \quad \widetilde{u} = \widetilde{w} = 0, \tag{6}$$

where U_s is the average wind speed at reference height z_s (= 300 m) in Hong Kong downtown. The domain ceiling and the lateral BCs are prescribed as symmetry. Both the building facades and ground surfaces are set to no-slip BCs. The free-stream velocity at the top boundary is $U_\infty = 10$ m s^{-1} and the maximum building height is $H_{max} = 180$ m. The Reynolds number Re ($= U_\infty H_{max}/\nu$) is, therefore, more than 10^8, fulfilling the independence from molecular viscosity. The mesh sensitivity was carried out in our previous work (Cheng *et al.*, 2021). Besides, a reduced-scale wind tunnel experiment (Mo *et al.*, 2021) was carried out to validate our LES results. No major difference in statistics is found in the comparison between LES and experiment (Yao *et al.*, 2022) or the change in resolution. In addition, the TBL height δ (=330 m), RSL top z_{RSL} (= 95 m), and ISL top z_{ISL} (= 228 m) of the whole computation domain are derived from our previous work.

III. THEORETICAL BACKGROUND

A. Scale decomposition and amplitude modulation

The signal of streamwise fluctuating velocities $u'(t)$ is decomposed into small-scale eddies ($\lambda_x < \delta$) and LSMs ($\lambda_x > \delta$) by a low-pass filter, where the wavelength λ_x is determined by Taylor hypothesis (Taylor, 1938). In general, small-scale eddies populate in the near-ground region, while the LSMs reside in the outer layer. In this study, the filter cutoff is at TBL thickness $\lambda_x = \delta$ that follows the suggestion of previous studies (Mathis *et al.*, 2009, Anderson, 2016, Tang *et al.*, 2019, and Kim *et al.*, 2020). The subscripts L and S denote, respectively, the large-scale

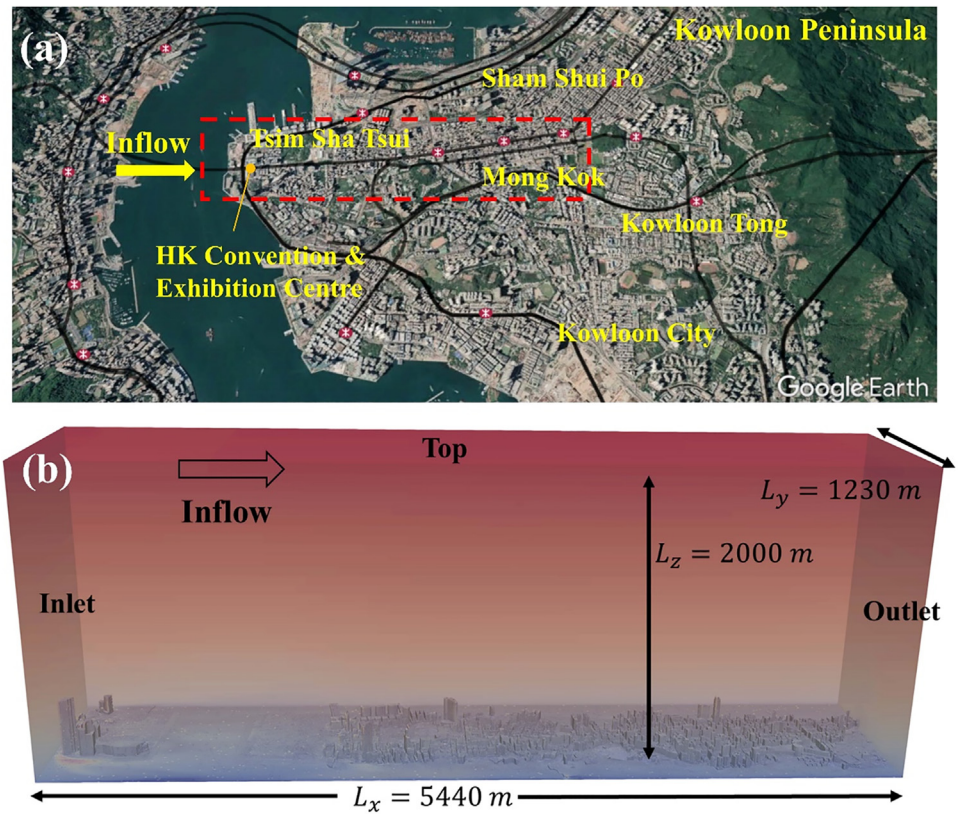

FIG. 1. (a) Satellite image of downtown Kowloon Peninsula, Hong Kong from Google Maps. (b) LES computation domain (Tsim Sha Tsui to Sham Shui Po).

$u_L'(t)$ and small-scale $u_S'(t)$ components of (the streamwise) fluctuating velocity.

AM describes how the large-scale flows (u_L') affect the amplitude of their small-scale counterpart (u_S'). The instantaneous amplitude of small-scale signal (u_S') is represented by its envelope $E(u_S')$, which is a smooth curve outlining the extremities of the oscillating signal. In the current case, the Hilbert transform (Huang *et al.*, 1998) is applied to extract the small-scale envelope $[E(u_S')]$ that is the most common approach adopted in the literature (Mathis *et al.*, 2009, Kim *et al.*, 2020). Next, the low-pass filter is applied to $E(u_S')$ to extract the large-scale time trace $[E_L(u_S'(t)]$ of the instantaneous amplitude of the high-frequency signal u_S'. According to Mathis *et al.* (2009) and Bernardini *et al.* (2011), the AM coefficient,

$$R_{AM} = \frac{\overline{u_L' E_L(u_S')}}{\sqrt{\overline{u_L'^2}}\sqrt{\overline{E_L(u_S')^2}}}, \tag{7}$$

measures the degree of small-scale eddies (u_S') being amplitude modulated by the large-scale ones (u_L'). It is noteworthy that the one-point AM coefficient (R_{AM}) in Eq. (7) provides a reasonable estimate of the full-range two-point R_{AM} (between near-ground and outer-layer regions; Mathis *et al.*, 2009, Bernardini *et al.*, 2011, and Kim *et al.*, 2020). Therefore, the one-point R_{AM} is exploited in this study to elaborate the inner–outer interaction across the ASL over real urban morphology.

B. Quadrant analysis and skewness factor

The turbulence signals in the streamwise u' and vertical w' direction can be partitioned into four quadrants (Table I). Among others, ejection Q_2 ($u' < 0$, $w' > 0$) and sweep Q_4 ($u' > 0$, $w' < 0$) contribute most to momentum flux ($u'w'$). On the other hand, outward interaction Q_1 and inward interaction Q_3 possess neglectable, negative contributions.

Skewness $(u'u'u')/(u'u')^{3/2}$ is commonly adapted to measure the degree of asymmetry of probability density function (PDF) of velocity signals (Ardeshiri *et al.*, 2020). In the current case, the asymmetry distribution of (the streamwise) fluctuating velocity can be measured by the skewness factor (Mathis *et al.*, 2011),

$$S_u = u'u'u', \tag{8}$$

which is essentially equivalent to skewness. Applying the scale decomposition $u' = u_L' + u_S'$, Eq. (8) is rewritten as

$$S_u = u_L'^3 + 3\left(u_L' u_S'^2 + u_L'^2 u_S'\right) + u_S'^3, \tag{9}$$

TABLE I. Quadrant events of momentum flux $u'w'$.

Q_1 (outward interaction)	$u' > 0$	$w' > 0$
Q_2 (ejection)	$u' < 0$	$w' > 0$
Q_3 (inward interaction)	$u' < 0$	$w' < 0$
Q_4 (sweep)	$u' > 0$	$w' < 0$

where ${u_L'}^3$, ${u_S'}^3$, and $3({u_L'}{u_S'}^2 + {u_L'}^2{u_S'})$ denote the asymmetry contribution from large scales, the asymmetry contribution from small scales, and the interaction between the large and small scales, respectively. For example, if the skewness factor $u'u'u' > 0$, more extremity resides in sweep Q_4 ($u' > 0$), so energetic eddy entrainment populates. By contrast, $u'u'u' < 0$ implies more extremity in ejection Q_2 ($u' < 0$), so burst events dominate.

IV. RESULT AND DISCUSSION

A. Premultiplied energy spectrum

Figure 2 depicts the shaded contours of premultiplied energy spectrum of streamwise fluctuating velocity $k_x\phi_{uu}/{u_\tau}^2$ as a function of streamwise wavelength λ_x/δ and elevation z. Here, k_x ($= 2\pi/\lambda_x$) is the streamwise wavenumber and ϕ_{uu} is the power spectrum of the streamwise fluctuating velocity (Moin, 2009, Squire *et al.*, 2017). In the RSL ($z < 95$ m), the streamwise TKE $u'u'$, which is mainly induced by the wall-attached eddies generated from the shear between the prevailing flows and the buildings (Marusic *et al.*, 2019, Hu *et al.*, 2020), concentrates in small scales ($\lambda_x < \delta$). By contrast, the energy is contributed prominently from long wavelength ($\lambda_x > \delta$) in the ISL and the outer layer that is mainly attributed to the well-developed VLSMs at high Reynolds stress (Tang *et al.*, 2016). The results agree well with their counterparts over smooth wall or idealized urban morphology (Ganapathisubramani *et al.*, 2012, Perret *et al.*, 2018, and Baars *et al.*, 2020). It is noteworthy that the contribution from LSMs is not negligible even in the RSL ($z < 95$ m). As such, the scale decomposition reported in Sec. III is applied to investigate the scale interaction between (small-scale) wall-attached eddies and LSMs.

B. Amplitude modulation

Figure 3 illustrates the one-point AM coefficient R_{AM} of the streamwise fluctuating velocity as a function of elevation z. The inner-scale and outer-scale are applied for normalization in Figs. 3(a) and 3(b), respectively. For inner scaling, the wall-normal distance from the smooth wall (Mathis *et al.*, 2009, Tang *et al.*, 2019) is presented in the wall unit z^+ ($= zu_\tau/\nu$). The elevation z over real-urban morphology is normalized by the rough-wall analogy $(z-d)/z_0$. Here, d is the zero-plane displacement, signifying the vertical shift in flows in

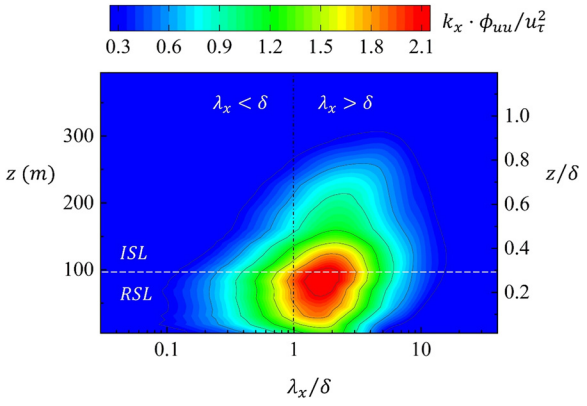

FIG. 2. Shaded contours of the premultiplied energy spectrum of streamwise fluctuating velocity $k_x\phi_{uu}/{u_\tau}^2$ plotted as functions of streamwise wavelength λ_x/δ and elevation z.

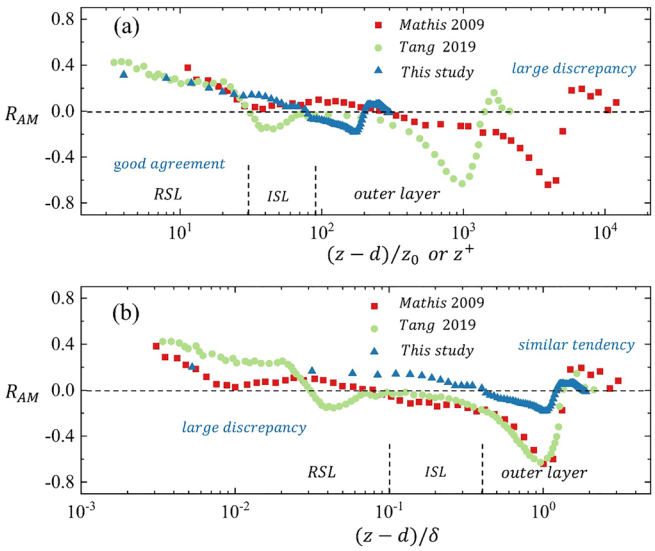

FIG. 3. Amplitude modulation coefficient of streamwise fluctuating velocity R_{AM} plotted against the elevation z normalized by (a) inner-scale z^+ for smooth wall (Mathis *et al.*, 2009, Tang *et al.*, 2019) and $(z - d)/z_0$ for the current case together with (b) outer-layer scaling $(z - d)/\delta$. Note that $d = 0$ for the smooth wall and $d > 0$ for rough wall (the current case).

response to the explicitly resolved roughness elements, and z_0 is the roughness height which is determined by the regression of the ISL log-law of the mean streamwise velocity profile. This analogy is commonly adopted in the comparison between smooth-wall and rough-wall results (Cui *et al.*, 2003, Leonardi *et al.*, 2007, Hultmark *et al.*, 2013, and Mo and Liu, 2018). For the regions away from the ground in the ISL and aloft, the outer-layer scaling $(z-d)/\delta$ is commonly used to compare the literature available for smooth walls ($d = 0$) and real-urban cases (rough walls; $d > 0$).

In the RSL ($z < 95$ m), the nonzero AM coefficient R_{AM} [Fig. 3(a)] provides a strong evidence that small-scale eddies associated with the underlying buildings are modulated by the LSMs (Schlatter *et al.*, 2010). The results are in good agreement with their smooth-wall counterparts (Mathis *et al.*, 2009, Tang *et al.*, 2019) under the inner scaling [Fig. 3(a)]. However, a large discrepancy is observed in the RSL under the outer scaling because of its inapplicability in the near-ground regions [Fig. 3(b)]. This also echoes the importance of proper selection of inner scale and outer scale in different ASL sublayers. In the RSL, the flows are largely influenced by the resistance (form drag and friction drag) from urban surface. Hence, the (dimensionless) inner scale that characterizes the surface features, such as roughness (z_0) and zero-plane displacement (d), works well in the cross-comparison among different cases. By contrast, the outer scale is characterized by a sufficiently large Reynolds number and fully developed turbulence that is seldom affected by individual roughness elements in the near-ground region. Therefore, the inner scale fails to give consistent results in the cross-comparison above the ISL.

The AM coefficient R_{AM} decreases with increasing elevation whose zero-crossing is close to the ISL top ($95 < z < 228$ m) under both inner scaling and outer scaling. This finding concurs with the previous work available in the literature (Mathis *et al.*, 2009,

Bernardini *et al.*, 2011, and Anderson, 2016). In the outer layer ($z > 228$ m), the tendency of R_{AM} over real-urban morphology is consistent with that of its smooth-wall counterpart under the outer-layer scaling [Fig. 3(b)]. However, the inner scaling fails to give a comparable result at that elevation [Fig. 3(a)]. Although all the three curves invariably reach their global minima at $(z-d) \approx \delta$ and local maxima at $(z-d) \approx 2\delta$, the current R_{AM} is slightly smaller in magnitude compared with its smooth-wall counterpart. The major reason could be the large difference in Reynolds number. The AM coefficient R_{AM} was shown to be an increasing function of the Reynolds number Re_τ $(=u_\tau\delta/\nu)$ at constant elevation (Yang *et al.*, 2017). The flows over smooth walls have been performed at finite Reynolds number ($Re_\tau = 2800$ for Mathis *et al.*, 2009 and $Re_\tau = 1024$ for Tang *et al.*, 2019). In the current flows over real urban morphology, the Reynolds number ($Re_\tau \geq 5 \times 10^6$) is much higher so uplifting R_{AM} could be observed.

Figure 4 compares the AM coefficient R_{AM} at different elevation z over a range of building layouts. The strongest R_{AM} is clearly observed in street canyons [$z = 50$ m; Fig. 4(a)]. Obviously, the downstream regions with dense buildings exhibit a strong R_{AM} (> 0.6) in support of a notable modulation mechanism, i.e., the positive (negative) large-scale velocity excursions induce local enhancement (suppression) of small-scale turbulent fluctuations (Bernardini *et al.*, 2011). However, the AM is weakened at higher elevations where the buildings are sparse [$z = 100$ and 200 m, respectively, on Figs. 4(b) and 4(c)]. It is also noteworthy that dissimilar AM patterns are depicted on the windward and leeward sides of a building (or building clusters). The AM coefficient R_{AM} tends to be negative and positive, respectively, on the windward sides and in building wakes. This finding suggests that the presence of buildings modifies the AM in the ASLs over urban areas in different manners.

Figure 5 presents the shaded contours of R_{AM} on the vertical x–z plane at different spanwise y locations. It is noteworthy that the wakes of upstream buildings (regardless of low-rise or high-rise) are always accompanied by positive R_{AM}. For example, some small wakes are initiated by low-rise buildings [Figs. 5(b), 5(d), and 5(e)] that illustrate the positive R_{AM} below a large area of negative R_{AM} in the upstream. By contrast, negative R_{AM} is observed mostly in the windward regions of high-rise buildings, especially near the rooftop associated with the local, fierce flow impingement. A few exceptionally tall buildings result in abrupt changes of building height that could modify the pressure and velocity significantly, promoting the RSL level substantially in the vertical (Cheng and Yang, 2023, Duan *et al.*, 2023). This could be one of the reasons for the dissimilar behavior of (negative) R_{AM} in the RSLs. Future work would be carried out to quantify the dynamical influence on R_{AM} by systematically controlling the changes in building height in idealized urban morphology.

Figure 6 contrasts the joint probability density function (JPDF) of dimensionless streamwise u'/u_τ and vertical w'/u_τ fluctuating velocities in regions with different amplitude modulation coefficient R_{AM}. The vertical extent is $50 \leq z \leq 150$ m.

Majority anisotropy and asymmetry of momentum flux ($u'w'$) are attributed to the large-scale components (u_L' and w_L'). Whilst, the

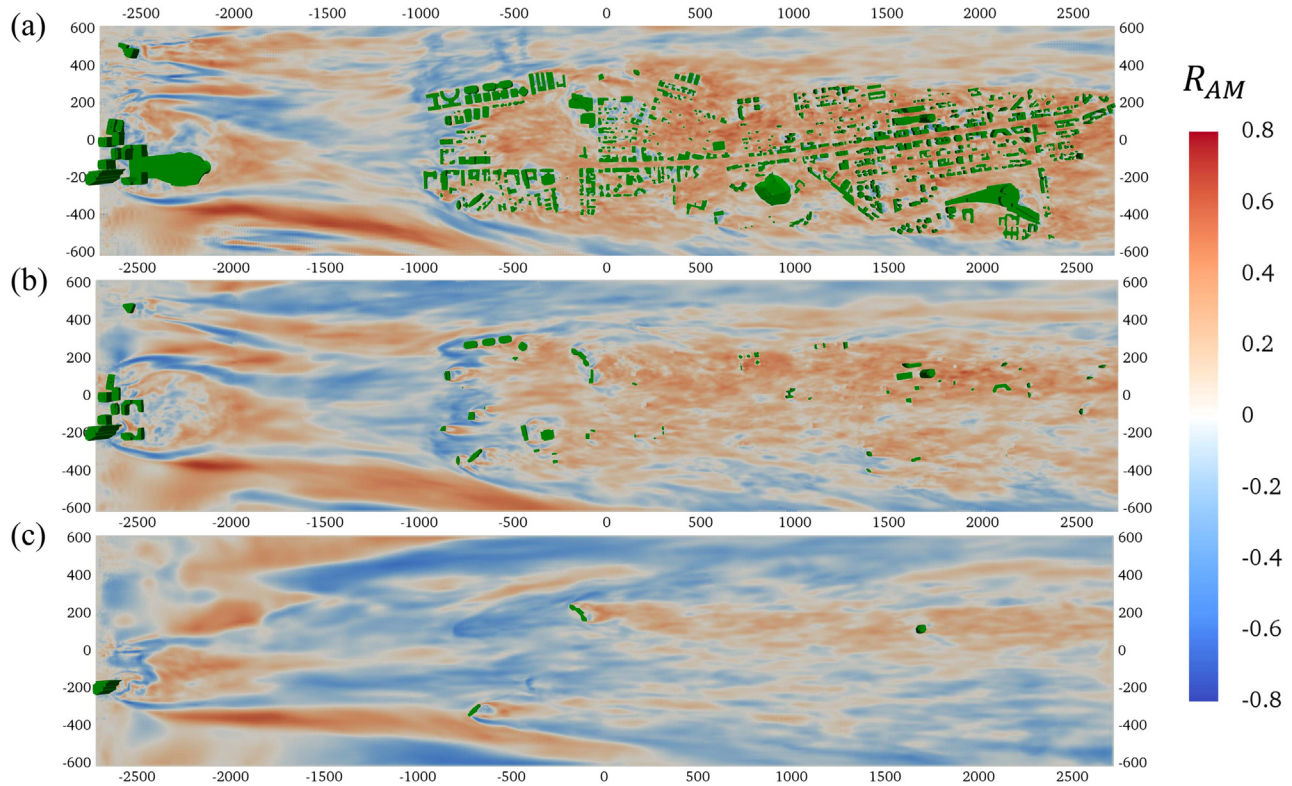

FIG. 4. Shaded contours of amplitude modulation coefficient R_{AM} in the horizontal x–y plane at $z =$ (a) 50 m, (b) 100 m, and (c) 200 m.

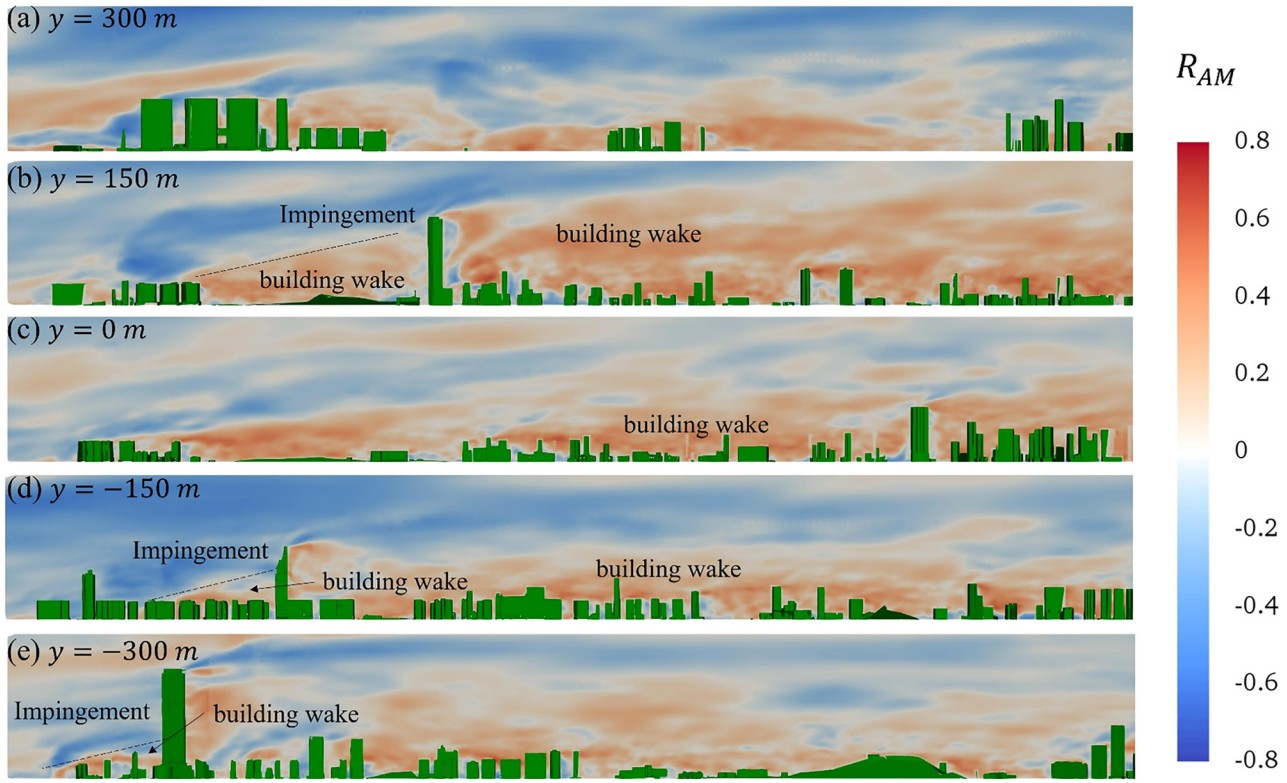

FIG. 5. Shaded contours of amplitude modulation coefficient R_{AM} in the vertical x–z plane at $y =$ (a) 300 m, (b) 150 m, (c) 0 m, (d) −150 m, and (e) −300 m.

small-scale components (u_S' and w_S') are rather isotropic (similar JPDF distribution in u' and w') and symmetric that echoes the Kolmogorov hypothesis (Kolmogorov, 1962). The symmetrically distributed small-scale eddies suggest relatively inefficient momentum transport (Fig. 6, last column). It is because the negative contribution from Q_1 and Q_3 offsets the positive contribution from Q_2 and Q_4. These small-scale eddies, in turn, shelter the flows in the street canyons (in the form of isotropy), weakening the momentum transport (and air exchange) with the outer layer. However, the predominant Q_2 and Q_4 from LSMs illustrate much more contribution than Q_1 and Q_3 (Fig. 6, second column), which are beneficial to turbulent transport.

From positive to negative R_{AM}, the mode of JPDF shifts from ejection (Q_2; $u' < 0$ and $w' > 0$) to sweep (Q_4; $u' > 0$ and $w' < 0$), while the most extreme events shift from sweep to ejection. This result indicates that the minority, strong ejection Q_2 dominates the transport in negative AM regions, while the strong Q_4 dominates the transport in widespread, positive AM regions. This result is consistent with the work of Mathis *et al.* (2011), in which R_{AM} was found rather consistent with the skewness of streamwise fluctuating velocity. For example, in the regions with $R_{AM} > 0.3$ [Fig. 6(a)], the JPDF mainly resides in negative u', while the extremities are in the positive u' regions, which could lead to positive streamwise skewness. In the region with $R_{AM} < -0.3$ [Fig. 6(d)], the majority shifts from positive to negative u', so the skewness turns negative. This finding also echoes our previous work (Mo *et al.*, 2021, Yao *et al.*, 2022) as well as other studies based on idealized urban morphology (Raupach, 1981, Zhu *et al.*, 2007) in which the large-scale, fast ($u' > 0$), downward ($w' < 0$) motions were found populating in the RSLs.

The skewness factor (S_u and S_w) and their components (large and small scales) are presented as functions of elevation $(z - d)/z_0$ in Fig. 7. They measure the asymmetry of distribution quantitatively. In the RSL, the positive S_u ($= u'u'u'$) and negative S_w ($= w'w'w'$) collectively illustrate that most of the extremities are in the form of sweep (Q_4; $u' > 0$ and $w' < 0$). This finding is consistent with the JPDF in those regions with widespread, positive R_{AM} [Fig. 6(b)]. In addition, the large-scale components ($u_L'u_L'u_L'$) and the scale interaction contribute equally to the streamwise asymmetry in the RSL. By contrast, in the ISL and the outer layer, the large-scale components account for most of the streamwise asymmetry, while the scale interaction diminishes. It is noteworthy that, in the vertical direction, the major asymmetry is attributed to the scale interaction.

In the ISL, on the other hand, the key contributors are the large-scale components. The small-scale components contribute insignificantly to asymmetry at all the elevations because they are isotropic according to the Kolmogorov hypothesis (Kolmogorov, 1962). Moreover, the attached eddies hypothesis (Townsend, 1976) assumes the wall-attached eddies to be Gaussian (zero skewness), which has been verified thoroughly (Baidya *et al.*, 2019, Marusic *et al.*, 2019, and Hu *et al.*, 2020). For example, Hu *et al.* (2020) demonstrated the existence of three kinds of RSL eddies: detached eddies (large-scale, major contributor to asymmetry), attached eddies (small-scale, Gaussian, skewness close to zero), and a few small-scale eddies detached from

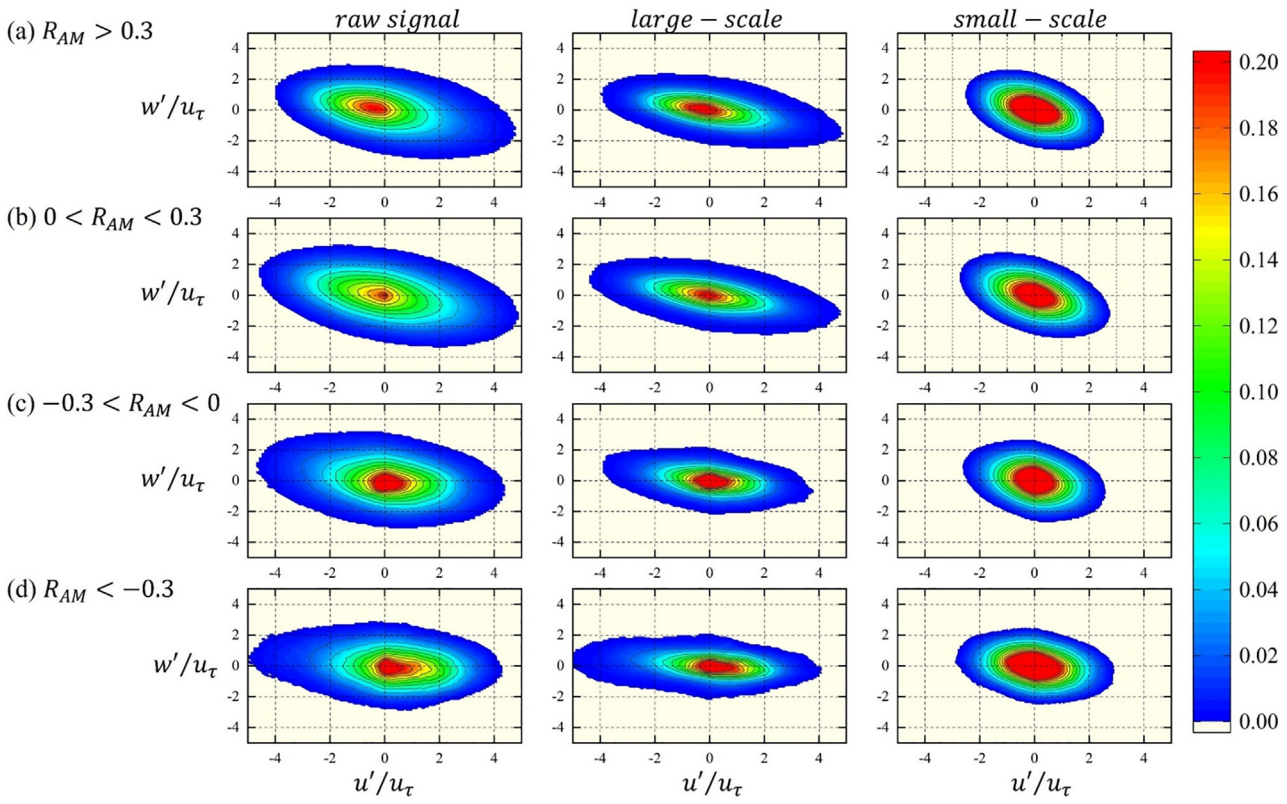

FIG. 6. Shaded contours of joint probability density function (JPDF) of dimensionless streamwise u'/u_τ and vertical w'/u_τ fluctuating velocities in regions with different R_{AM}. (a) $R_{AM} > 0.3$, (b) $0 < R_{AM} < 0.3$, (c) $-0.3 < R_{AM} < 0$, and (d) $R_{AM} < -0.3$. From left to right: raw signal, large-scale component, and small-scale component, respectively.

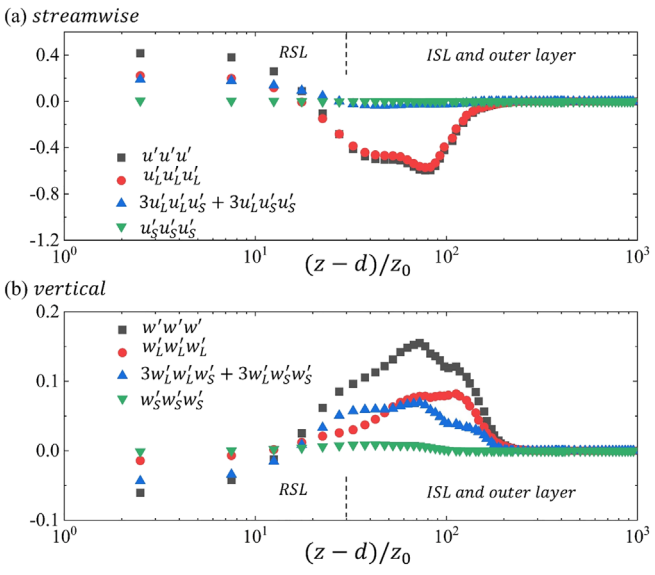

FIG. 7. Skewness factors of (a) streamwise S_u $(= u'u'u')$ and (b) vertical S_w $(=w'w'w')$ velocities plotted as functions of elevation $(z-d)/z_0$.

the wall, whose symmetry cannot be guaranteed. In the current work, the building facades provide much more additional surface area than smooth-wall configurations, promoting the attached eddies in the small-scale eddies. In this connection, the small-scale eddies seldom contribute to the RSL asymmetry.

In summary, the isotropic, small-scale eddies populate in the RSL. Whilst the anisotropic large-scale eddies populate in the ISL and outer layer. The RSL flows become anisotropic mainly due to the entrainment of large-scale eddies together with the interaction between the large-scale and small-scale motions.

C. Conditional sampling

Figure 8(a) illustrates the small-scale streamwise TKE portion deviation from the mean $\bar{S}$ $(= \overline{u_s'u_s'}/\overline{u'u'})$ under large-scale acceleration $(u_L' > 0)$ and large-scale deceleration $(u_L' < 0)$ via conditional sampling in time domain. The horizontal x–y plane at the street-canyon level (RSL; $z = 50$ m) is shown. The solid yellow lines and solid black lines denote the contours for $R_{AM} = 0.2$ and -0.2, respectively. In addition, the detailed views on the vertical x–z plane at different spanwise locations ($y = 150$, 0, and -150 m) are also presented in Fig. 9(a).

Figures 8(a) and 9(a) show a striking similarity to the spatial distribution of AM coefficient R_{AM}. When large-scale

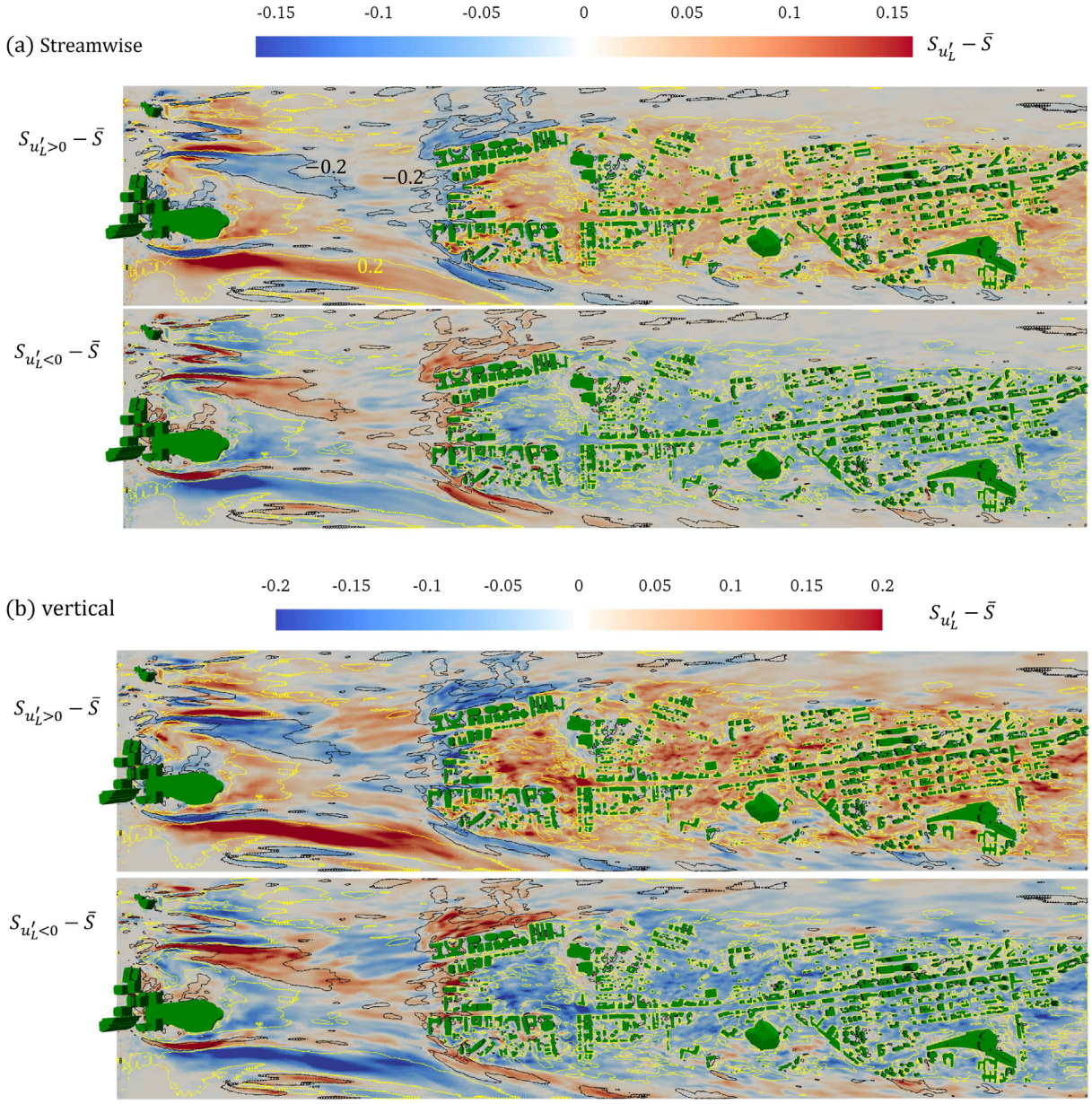

FIG. 8. (a) Shaded contours of small-scale streamwise TKE portion deviation from the mean $\bar{S}$ ($= \overline{u_S' u_S'}/\overline{u'u'}$) under large-scale acceleration ($u_L' > 0$) and large-scale deceleration ($u_L' < 0$). The yellow contour line denotes $R_{AM} = 0.2$, and the black contour line denotes $R_{AM} = -0.2$. (b) Shaded contours of small-scale vertical TKE portion deviation from the mean $\bar{S}$ ($= \overline{w_S' w_S'}/\overline{w'w'}$) under large-scale acceleration ($u_L' > 0$) and large-scale deceleration ($u_L' < 0$). The yellow and black contour line denotes $R_{AM} = 0.2$ and $R_{AM} = -0.2$, respectively.

acceleration ($u_L' > 0$; usually associated with sweep $Q4$) is passing by, small-scale eddies exhibit an energy surplus in positive AM regions in the street canyons but an energy deficit in the negative AM regions. By contrast, the passage of large-scale deceleration ($u_L' < 0$; usually associated with sweep Q_2) subsequently decreases the small-scale TKE portion in the positive AM regions but increases in the negative AM regions. This result is also consistent with that in Kim *et al.* (2020), which reported that the LSMs of high-momentum ($u_L' > 0$) and low-momentum ($u_L' < 0$) flows lead to the small-scale energy surplus and deficit, respectively, in permeable rough walls.

Unlike smooth walls or idealized urban morphology (regular layout), in the RSLs (street canyons) over real urban morphology, the regions with negative R_{AM} are mainly induced by the heterogeneous building layout. This once again stresses the advantage and importance of building-resolved LES on complex urban morphology as well as the near-ground flows and dynamics.

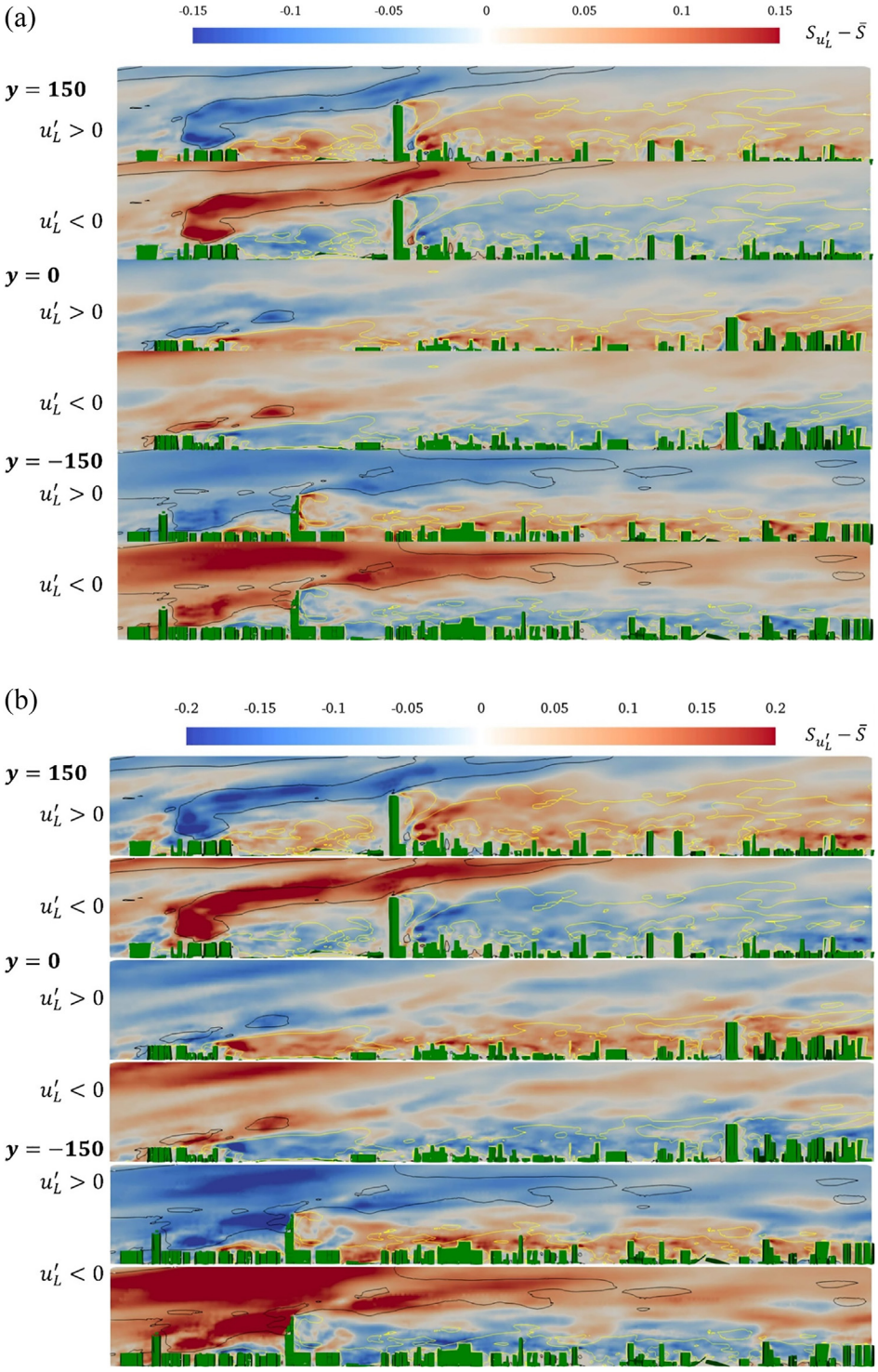

FIG. 9. (a) Detailed shaded contours of small-scale streamwise TKE portion deviation from the mean $\bar{S}$ $(= \overline{u_S' u_S'}/\overline{u'u'})$ under large-scale acceleration $(u_L' > 0)$ and large-scale deceleration $(u_L' < 0)$. The yellow and black contour lines denote $R_{AM} = 0.2$ and $R_{AM} = -0.2$, respectively. (b) Detailed shaded contours of small-scale vertical TKE portion deviation from the mean $\bar{S}$ $(= \overline{w_s' w_s'}/\overline{w'w'})$ under large-scale acceleration $(u_L' > 0)$ and large-scale deceleration $(u_L' < 0)$. The yellow and black contour lines denote $R_{AM} = 0.2$ and $R_{AM} = -0.2$, respectively.

Figures 8(b) and 9(b) illustrate the small-scale vertical TKE portion deviation from the mean $\bar{S}$ $(= \overline{w_s' w_s'}/\overline{w'w'})$ under large-scale accelerating $(u_L' > 0)$ and decelerating $(u_L' < 0)$ flows. Similar to its streamwise counterpart [Figs. 8(a) and 9(a)], the energy surplus/deficit of small-scale vertical motions $(w_S' w_S')$ appears at the passage of large-scale sweep $Q4$ and ejection $Q2$ events in the positive R_{AM} zones. While in the negative R_{AM} zones, the passages of sweep $Q4$ and ejection $Q2$ induce energy deficit and surplus, respectively, to the small-scale

TABLE II. Correlation between large-scale turbulence structure and small-scale TKE.

	$R_{AM} > 0$		$R_{AM} < 0$	
Large-scale events	$Q4$ (dominant)	$Q2$	$Q2$ (dominant)	$Q4$
Fluctuation direction	$u_L' > 0$	$u_L' < 0$	$u_L' < 0$	$u_L' > 0$
Small-scale amplitude	Increase	Decrease	Increase	Decrease
Small-scale TKE	Increase	Decrease	Increase	Decrease

eddies. Evidently, the streamwise and vertical fluctuating velocities share the same AM patterns that are both subject to the AM by large-scale streamwise fluctuating velocity u_L' (Talluru *et al.*, 2014).

Although the zones with negative and positive R_{AM} are dominated by different flow patterns (Q_2 and Q_4), the LSMs influence the small-scale TKE similarly. It is because they both increase the small-scale TKE by increasing the amplitude of small-scale eddies (Table II). In other words, the presence of the LSMs increases the small-scale TKE (turbulence intensity) that subsequently promotes the local transport.

Figure 10 illustrates a schematic diagram summarizing the AM in the ASLs over real urban morphology, as revealed by the results presented herein. The large-scale sweeps $Q4$ and ejections $Q2$ are anisotropic/asymmetric, so they are effective in transport. In contrast, small-scale eddies are isotropic/symmetric that shelter the street canyons from the outer-layer flows. Most zones in street canyons (RSL) are subject to positive AMs in which the transport processes are mainly governed by large-scale sweep $Q4$. Its passage results in a small-scale energy surplus locally. While, the passage of ejection $Q2$ leads to small-scale energy deficits. However, there exist some zones (mainly the windward side of the buildings) which are subject to negative AM so the transport is driven by large-scale ejection $Q2$. In short, the passage of ejection $Q2$ and sweep Q4 leads to small-scale energy deficits and surplus, respectively, over real urban morphology.

V. PRACTICAL IMPLICATION

Although the LSMs are characterized by favorable transport efficiency and remarkable energy, their utilization (for pedestrian-level health and safety) is rather limited. Focusing on the ASL, this paper investigates how the LSMs in the outer layer modulate the small-scale eddies in the street canyons over a range of urban morphology, paving the avenue to the transport enhancement by LSMs with proper urban planning, achieving a sustainable living environment in the modern metropolis.

First of all, LSMs, regardless of the sight of the AM coefficient R_{AM} (positive or negative), excite the small-scale eddies in street canyons, modifying the local transport performance. Apart from promoting pedestrian-level winds, AM provides an alternative solution to improve pedestrian-level air quality by generating more large-scale turbulence through controlling the design, such as shape, height, and orientation, of new buildings properly. New development projects could be evaluated in the design stage to initiate more turbulence by refining the architectural design.

Second, near-ground regions are mostly dominated by sweep Q4 (fresh air entrainment) that are favorable for landuse with residential buildings and schools. By contrast, negative AM zones are governed by ejection $Q2$ that is appropriate for landuse with hazardous materials, such as power plants and waste treatment, to avoid re-entrainment of emitted pollutants. With the proper selection in the positive AM regions, the pedestrian-level air quality could be improved by enhancing the AM through architectural design or urban planning, realizing a sustainable living environment in the metropolis.

Furthermore, AM (either negative or positive R_{AM}) enhances the small-scale eddies in street canyons which directly affect the mixing of chemically reactive pollutants, such as vehicular exhaust nitric oxide (NO) and ozone (O_3). There is no doubt that its influence on chemically reactive pollutant transport in street canyons is worthy of further investigation.

VI. CONCLUSIONS

In this paper, we critically examined the AM in the ASLs over real urban morphology. Similar to its smooth-wall counterpart, most

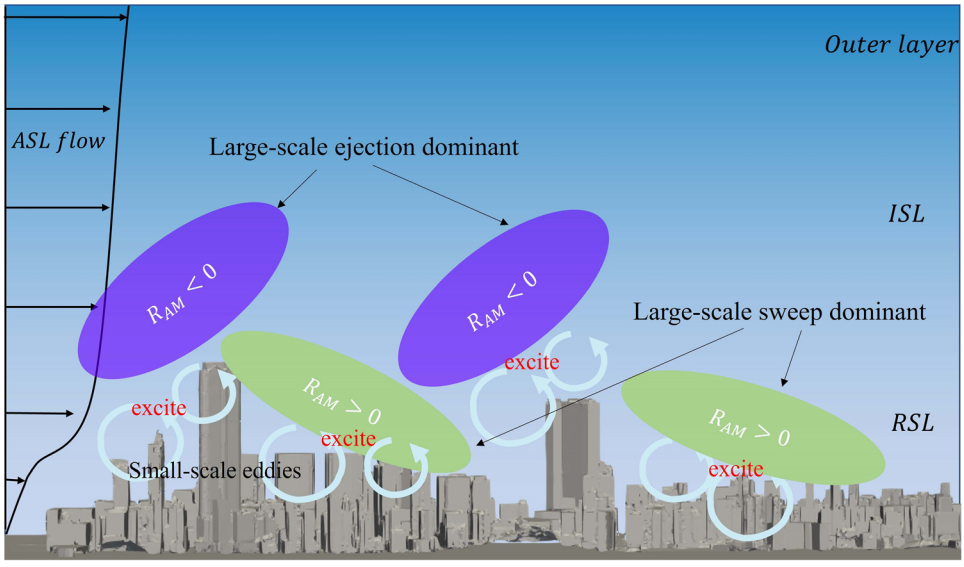

FIG. 10. Schematic summarizes the inner–outer-layer interaction in real-urban ASL as revealed by the results presented herein.

near-ground regions (RSLs) exhibit a positive AM coefficient $R_{AM} > 0$. Evidently, the small-scale turbulence structures in street canyons are modulated by the outer-layer LSMs. In addition, different building configurations are found to affect AM significantly. In this study, negative AM, $R_{AM} < 0$, is unprecedentedly found in the RSL on the windward side of buildings, illustrating the influence of heterogeneous building surfaces and flow dynamics together with the unique results in the presence of explicitly resolved buildings. It is obviously one of the key advantages of resolving buildings explicitly in LESs compared with empirical RSL modeling or even Reynolds-averaged Navier–Stokes (RANS) turbulence models.

A range of dominant turbulence structures are found in zones with positive or negative AM. In the zones with positive AM, large-scale sweep $Q4$ dominates, increasing the small-scale TKE in the street canyons. However, the infrequent passage of large-scale ejection $Q2$ tends to reduce the small-scale TKE locally. By contrast, in zones with negative AM, large-scale ejection $Q2$ dominates the transport, increasing the small-scale TKE in the street canyon. Whereas, the infrequent passage of large-scale sweep tends to reduce the small-scale TKE there.

In addition, majority flow anisotropy and asymmetry are initiated by the large-scale velocity components together with the scale interaction between large- and small-scale eddies. The small-scale eddies are rather weak in momentum transport, sheltering the street-canyon flows from the outer-layer dynamics aloft. Moreover, their positive ($Q2$ and $Q4$) and negative ($Q1$ and $Q3$) contributions to momentum flux offset each other. This finding consistently illustrates the significance of LSM entrainment in improving local transport processes.

ACKNOWLEDGMENTS

This research is conducted, in part, using the research computing facilities and/or advisory services offered by Information Technology Services (ITS), The University of Hong Kong (HKU). Technical support from Ms. L. Y. L. Chan, Mr. W. K. Kwan, and Mr. B. H. T. Yau is appreciated. This study is partly supported by the Hong Kong (HK) Research Grants Council (RGC) Theme-based Research Scheme (TRS) No. T24–504/17-N, the HK RGC Collaborative Research Fund (CRF) Nos. C7064 18G and C5108 20G, as well as the HK RGC General Research Fund (GRF) Nos. 17209819 and 17211322.

AUTHOR DECLARATIONS

Conflict of Interest

The authors have no conflicts to disclose.

Author Contributions

Yixun Liu: Data curation (equal); Formal analysis (equal); Investigation (equal); Methodology (equal); Software (equal); Validation (equal); Visualization (equal); Writing – original draft (equal). **Chun-Ho Liu:** Conceptualization (equal); Funding acquisition (equal); Project administration (equal); Resources (equal); Supervision (equal); Writing – review & editing (equal). **Guy P. Brasseur:** Funding acquisition (equal); Methodology (equal); Writing – review & editing (equal). **Christopher Chao:** Funding acquisition (equal); Methodology (equal); Writing – review & editing (equal).

DATA AVAILABILITY

The data that support the findings of this study are available from the corresponding author upon reasonable request.

REFERENCES

Agostini, L. *et al.*, "The Impact of footprints of large-scale uuter structures on the near-wall layer in the presence of drag-reducing spanwise wall motion," Flow Turbul. Combust. **100**(4), 1037–1061 (2018).
Ahmadi-Baloutaki, M. *et al.*, "A very large eddy simulation model using a reductionist inlet turbulence generator and wall modeling for stable atmospheric boundary layers," Fluid Dyn. **56**(3), 413–432 (2021).
Aliabadi, A. A. *et al.*, "A very large-eddy simulation (VLES) model for the investigation of the neutral atmospheric boundary layer," J. Wind Eng. Ind. Aerodyn. **183**, 152–171 (2018).
Aliabadi, A. A. *et al.*, "Flow and temperature dynamics in an urban canyon under a comprehensive set of wind directions, wind speeds, and thermal stability conditions," Environ. Fluid Mech. **19**(1), 81–109 (2019).
Alirol, E. *et al.*, "Urbanisation and infectious diseases in a globalised world," Lancet Infect. Dis. **11**(2), 131–141 (2011).
Anderson, W., "Amplitude modulation of streamwise velocity fluctuations in the roughness sublayer: Evidence from large-eddy simulations," J. Fluid Mech. **789**, 567–588 (2016).
Ardeshiri, H. *et al.*, "On the convergence and capability of the large-eddy simulation of concentration fluctuations in passive plumes for a neutral boundary layer at infinite Reynolds number," Boundary Layer Meteorol. **176**(3), 291–327 (2020).
Auvinen, M. *et al.*, "Study of realistic urban boundary layer turbulence with high-resolution large-eddy simulation," Atmosphere **11**(2), 201 (2020).
Baars, W. J. *et al.*, "Data-driven decomposition of the streamwise turbulence kinetic energy in boundary layers. I. Energy spectra," J. Fluid Mech. **882**, A25 (2020).
Baidya, R. *et al.*, "Simultaneous skin friction and velocity measurements in high Reynolds number pipe and boundary layer flows," J. Fluid Mech. **871**, 377–400 (2019).
Bandyopadhyay, P. R. *et al.*, "Structure of rough-wall turbulent boundary layers," Phys. Fluids (1958) **31**(7), 1877–1883 (1988).
Barlow, J. F., "Progress in observing and modelling the urban boundary layer," Urban Clim. **10**, 216–240 (2014).
Bernardini, M. *et al.*, "Inner/outer layer interactions in turbulent boundary layers: A refined measure for the large-scale amplitude modulation mechanism," Phys. Fluids **23**(6), 061701 (2011).
Bernardini, M. *et al.*, "Velocity statistics in turbulent channel flow up to $Re_\tau = 4000$," J. Fluid Mech. **742**, 171–191 (2014).
Bisset, D. K. *et al.*, "Topology and transport properties of large-scale organized motion in a slightly heated rough wall boundary layer," Phys. Fluids. A **3**(9), 2220–2228 (1991).
Bross, M. *et al.*, "Interaction of coherent flow structures in adverse pressure gradient turbulent boundary layers," J. Fluid Mech. **873**, 287–321 (2019).
Cheng, W. C., Liu, C.-H., Ho, Y.-K., Mo, Z., Wu, Z., Li, W., Chan, L. Y. L., Kwan, W. K., and Yau, H. T., "Turbulent flows over real heterogeneous urban surfaces: Wind tunnel experiments and Reynolds-averaged Navier-Stokes simulations," Build. Simul. **14**(5), 1345–1358 (2021).
Cheng, W.-C. and Yang, Y., "Scaling of flows over realistic urban geometries: A large-eddy simulation study," Boundary Layer Meteorol. **186**, 125–144 (2023).
Coceal, O. *et al.*, "Structure of turbulent flow over regular arrays of cubical roughness," J. Fluid Mech. **589**, 375–409 (2007).
Corino, E. R. *et al.*, "A visual investigation of the wall region in turbulent flow," J. Fluid Mech. **37**(1), 1–30 (1969).
Cui, J. *et al.*, "Large-eddy simulation of turbulent flow in a channel with rib roughness," Int. J. Heat Fluid Flow **24**(3), 372–388 (2003).
Deardorff, J. W., "A numerical study of three-dimensional turbulent channel flow at large Reynolds numbers," J. Fluid Mech. **41**(2), 453–480 (1970).
Duan, G. *et al.*, "Impacts of urban morphometric indices on ventilation," Build. Environ. **229**, 109907 (2023).
Farkas, Á. *et al.*, "Effects of hygroscopic growth of ambient urban aerosol particles on their modelled regional and local deposition in healthy and COPD-

compromised human respiratory system," Sci. Total Environ. **806**, 151202 (2022).
Forouzanfar, M. H. *et al.*, "Global, regional, and national comparative risk assessment of 79 behavioural, environmental and occupational, and metabolic risks or clusters of risks, 1990–2015: A systematic analysis for the global burden of disease study 2015," Lancet **388**(10053), 1659–1724 (2016).
Ganapathisubramani, B. *et al.*, "Amplitude and frequency modulation in wall turbulence," J. Fluid Mech. **712**, 61–91 (2012).
Giometto, M. G. *et al.*, "Spatial characteristics of roughness sublayer mean flow and turbulence over a realistic urban surface," Boundary Layer Meteorol. **160**(3), 425–452 (2016).
Hu, R. *et al.*, "Wall-attached and wall-detached eddies in wall-bounded turbulent flows," J. Fluid Mech. **885**, A30 (2020).
Huang, N. E. *et al.*, "The empirical mode decomposition and the Hilbert spectrum for nonlinear and non-stationary time series analysis," Proc. R. Soc. London, Ser. A **454**(1971), 903–995 (1998).
Hultmark, M. *et al.*, "Logarithmic scaling of turbulence in smooth- and rough-wall pipe flow," J. Fluid Mech. **728**, 376–395 (2013).
Hutchins, N. *et al.*, "Evidence of very long meandering features in the logarithmic region of turbulent boundary layers," J. Fluid Mech. **579**, 1–28 (2007a).
Hutchins, N. *et al.*, "Large-scale influences in near-wall turbulence," Philos. Trans. R. Soc. A **365**(1852), 647–664 (2007b).
Inagaki, A. *et al.*, "A numerical study of turbulence statistics and the structure of a spatially-developing boundary layer over a realistic urban geometry," Boundary Layer Meteorol. **164**(2), 161–181 (2017).
Kim, T. *et al.*, "Experimental evidence of amplitude modulation in permeable-wall turbulence," J. Fluid Mech. **887**, A3 (2020).
Kline, S. J. *et al.*, "The structure of turbulent boundary layers," J. Fluid Mech. **30**(4), 741–773 (1967).
Kolmogorov, A. N., "A refinement of previous hypotheses concerning the local structure of turbulence in a viscous incompressible fluid at high Reynolds number," J. Fluid Mech. **13**(1), 82–85 (1962).
Lee, V. J. *et al.*, "Epidemic preparedness in urban settings: New challenges and opportunities," Lancet Infect. Dis. **20**(5), 527–529 (2020).
Leonardi, S. *et al.*, "Properties of d- and k-type roughness in a turbulent channel flow," Phys. Fluids **19**(12), 125101 (2007).
Li, Q. *et al.*, "Contrasts between momentum and scalar transport over very rough surfaces," J. Fluid Mech. **880**, 32–58 (2019).
Li, X. *et al.*, "Turbulent/Synoptic separation and coherent structures in the atmospheric surface layer for a range of surface roughness," Boundary Layer Meteorol. **182**(1), 75–93 (2021).
Lin, H. B. *et al.*, "Spectral characteristics of surface atmosphere in range of macroscale to microscale at Hong Kong," J. Wind Eng. Ind. Aerodyn. **208**, 104446 (2021).
Liu, Y., Liu, C.-H., Brasseur, G. P., and Chao, C. Y. H., "Proper orthogonal decomposition of large-eddy simulation data over real urban morphology," Sustainable Cities Soc. **89**, 104324 (2023a).
Liu, Y., Liu, C.-H., Brasseur, G. P., and Chao, C. Y. H., "Wavelet analysis of the atmospheric flows over real urban morphology," Sci. Total Environ. **859**(1), 160209 (2023b).
Lotfy, E. R. *et al.*, "Characteristics of turbulent coherent structures in atmospheric flow under different shear–buoyancy conditions," Boundary Layer Meteorol. **173**(1), 115–141 (2019).
Lu, S. *et al.*, "Measurements of the structure of the Reynolds stress in a turbulent boundary layer," J. Fluid Mech. **60**(3), 481–511 (1973).
Marusic, I. *et al.*, "Attached eddy model of wall turbulence," Annu. Rev. Fluid Mech. **51**(1), 49–74 (2019).
Mathis, R. *et al.*, "Large-scale amplitude modulation of the small-scale structures in turbulent boundary layers," J. Fluid Mech. **628**, 311–337 (2009).
Mathis, R. *et al.*, "The relationship between the velocity skewness and the amplitude modulation of the small scale by the large scale in turbulent boundary layers," Phys. Fluids **23**(12), 121702 (2011).
Mo, Z. and Liu, C.-H., "A wind tunnel study of ventilation mechanism over hypothetical urban roughness: The role of intermittent motion scales," Build. Environ. **135**, 94–103 (2018).
Mo, Z., Liu, C.-H., and Ho, Y.-K., "Roughness sublayer flows over real urban morphology: A wind tunnel study," Build. Environ. **188**, 107463 (2021).
Moin, P., "Revisiting Taylor's hypothesis," J. Fluid Mech. **640**, 1–4 (2009).
OpenFOAM (2022). https://openfoam.org/.
Perret, L. *et al.*, "Large-scale structures over a single street canyon immersed in an urban-type boundary layer," Boundary Layer Meteorol. **148**(1), 111–131 (2013).
Perret, L. *et al.*, "The atmospheric boundary layer over urban-like terrain: Influence of the plan density on roughness sublayer dynamics," Boundary Layer Meteorol. **170**(2), 205–234 (2018).
Pope, S. B. *et al.*, *Turbulent Flows* (Cambridge University Press, 2000).
Raupach, M., "Conditional statistics of Reynolds stress in rough-wall and smooth-wall turbulent boundary layers," J. Fluid Mech. **108**, 363–382 (1981).
Reuther, N. *et al.*, "Effect of the intermittency dynamics on single and multipoint statistics of turbulent boundary layers," J. Fluid Mech. **897**, A11 (2020).
Rowe, B. R. *et al.*, "Simple quantitative assessment of the outdoor versus indoor airborne transmission of viruses and COVID-19," Environ. Res. **198**, 111189 (2021).
Salesky, S. *et al.*, "Buoyancy effects on large-scale motions in convective atmospheric boundary layers: Implications for modulation of near-wall processes," J. Fluid Mech. **856**, 135–168 (2018).
Schlatter, P. *et al.*, "Quantifying the interaction between large and small scales in wall-bounded turbulent flows: A note of caution," Phys. Fluids **22**(5), 051704 (2010).
Shrivastava, S. *et al.*, "Preventing diseases through promotion of a healthier environment: World health organization," Ann. Trop. Med. Public Health **9**(5), 364–365 (2016).
Smagorinsky, J., "General circulation experiments with the primitive equations. I. The basic experiment," Mon. Weather Rev. **91**(3), 99–164 (1963).
Spalding, D. B., "A new analytical expression for the drag of a flat plate valid for both the turbulent and laminar regimes," Int. J. Heat Mass Transfer **5**(12), 1133–1138 (1962).
Squire, D. T. *et al.*, "Applicability of Taylor's hypothesis in rough- and smooth-wall boundary layers," J. Fluid Mech. **812**, 398–417 (2017).
Talluru, K. M. *et al.*, "Amplitude modulation of all three velocity components in turbulent boundary layers," J. Fluid Mech. **746**, R1 (2014).
Tang, Z. *et al.*, "Bursting process of large- and small-scale structures in turbulent boundary layer perturbed by a cylinder roughness element," Exp. Fluids **57**(5), 79 (2016).
Tang, Z. *et al.*, "Scale interaction and arrangement in a turbulent boundary layer perturbed by a wall-mounted cylindrical element," Phys. Fluids **30**(5), 055103 (2018).
Tang, Z. *et al.*, "Local dynamic perturbation effects on amplitude modulation in turbulent boundary layer flow based on triple decomposition," Phys. Fluids **31**(2), 025120 (2019).
Taylor, G. I., "The spectrum of turbulence," Proc. R. Soc. London, Ser. A **164** (919), 476–490 (1938).
Tominaga, Y., *et al.* "AIJ guidelines for practical applications of CFD to pedestrian wind environment around buildings," J. Wind Eng. Ind. Aerodyn. **96**(10), 1749–1761 (2008).
Townsend, A. A., *The Structure of Turbulent Shear Flow* (Cambridge University Press, Cambridge, 1976).
Vinuesa, R. *et al.*, "Convergence of numerical simulations of turbulent wall-bounded flows and mean cross-flow structure of rectangular ducts," Meccanica (Milan) **51**(12), 3025–3042 (2016).
Wang, W. *et al.*, "On the correlation of water vapor and CO_2: Application to flux partitioning of evapotranspiration," Water Resour. Res. **52**(12), 9452–9469, https://doi.org/10.1002/2015WR018161 (2016).
Wu, S., Christensen, K., and Pantano, C., "A study of wall shear stress in turbulent channel flow with hemispherical roughness," J. Fluid Mech. **885**, A16 (2020).
Yang, X. I. A. *et al.*, "Implication of Taylor's hypothesis on measuring flow modulation," J. Fluid Mech. **836**, 222–237 (2017).
Yao, L., Liu, C.-H., Mo, Z., Cheng, W.-C., Brasseur, G. P., and Chao, C. Y. H., "Statistical analysis of the organized turbulence structure in the inertial and roughness sublayers over real urban area by building-resolved large-eddy simulation," Build. Environ. **207**, 108464 (2022).
Yoshizawa, A. *et al.*, "A statistically-derived subgrid-scale kinetic energy model for the large-eddy simulation of turbulent flows," J. Phys. Soc. Jpn. **54**(8), 2834–2839 (1985).
Zhu, W. *et al.*, "PIV measurements in the atmospheric boundary layer within and above a mature corn canopy. II. Quadrant-hole analysis," J. Atmos. Sci. **64**(8), 2825–2838 (2007).